GMR
The Original

GREEN SYNTHESIZED COPPER OXIDE NANOPARTICLES INCORPORATED WITH STARCH POLYVINYL ALCOHOL ELECTROSPUN NANOSCAFFOLDS EXHIBIT ENHANCED ANTIMICROBIAL ACTIVITY

Vinuritha Kandaswamy[1], Anoosh Golla[2], Narasimhalu CRV[3], Alagendran Subbarayalu[4], Kaliyamoorthy Dass[5*]

[1]Saveetha Medical College & Hospital (SMCH), Saveetha Institute of Medical and Technical Sciences (SIMATS), Thandalam, Chennai, Tamil Nadu 602105, India. Email: vinu.kandha5@gmail.com
[2]Department of Neurology, Saveetha Medical College and Hospital, Saveetha Institute of Medical And Technical Sciences (SIMATS), Thandalam, Chennai-602105, Tamil Nadu, India. Email: anushyadav2025@gmail.com.
[3]Department of Dermatology, Saveetha Medical College and Hospital, Saveetha Institute of Medical And Technical Sciences (SIMATS), Thandalam, Chennai-602105, Tamil Nadu, India. Email: narasimhalucrv.smc@saveetha.com; ORCID: https://orcid.org/0009-0005-8261-5512
[4]Saveetha College of Nursing (SCON), Saveetha Institute of Medical and Technical Sciences (SIMATS), Chennai – 602105, Tamil Nadu, India. Email: alagendrans.scon@saveetha.com; ORCID: https://orcid.org/0009-0009-0749-7180
[5*]Natural Product and Vector Control Research Lab, Department of Pharmacology, Saveetha Medical College and Hospital, Saveetha Institute of Medical And Technical Sciences (SIMATS), Thandalam, Chennai-602105, Tamil Nadu, India. Email: dass.smc@saveetha.com; ORCID: https://orcid.org/0000-0002-4564-3275

ABSTRACT

This study investigates the green synthesis, characterization, and antimicrobial efficacy of *Ectocarpales* algal extract-mediated copper oxide nanoparticles (CuO NPs) loaded starch/PVA electrospun nanoscaffolds. UV-Visible spectroscopy confirmed the distinct optical properties of the algal extract (absorption peak at 300 nm, indicating π-π* transitions) and CuO NPs (sharp peak at 200 nm, signifying surface plasmon resonance). Fourier-transform infrared spectroscopy (FT-IR) analysis revealed characteristic functional groups, including Cu–O bonds (860 cm^{-1}) in CuO NPs and polymer-related vibrations (1652 cm^{-1}, C=O stretching) in nanoscaffolds. X-ray diffraction (XRD) confirmed the monoclinic tenorite phase of CuO NPs (25 diffraction peaks) and semi-crystalline nature of nanoscaffolds (14 peaks). Scanning electron microscopy (SEM) imaging showed spherical CuO NPs and porous, fibrous nanoscaffolds with embedded NPs. Thermogravimetric analysis (TGA) indicated thermal stability, with nanoscaffolds exhibiting 31.1% weight loss up to 400°C. Zeta potential analysis demonstrated moderate colloidal stability (+14.03 mV). Antimicrobial assays revealed superior efficacy of nanoscaffolds against bacterial (E. coli, S. aureus) and fungal (A. niger, Penicillium spp.) pathogens compared to algal extract and CuO NPs alone. These findings highlight the potential of biosynthesized CuO NP-integrated nanoscaffolds for biomedical applications due to their structural integrity, thermal resilience, and enhanced antimicrobial performance.

KEYWORDS: *Ectocarpales*, Green synthesis, CuO Nanoparticles, Starch/PVA Nanoscaffolds, Antimicrobial Activity.

1. INTRODUCTION

Nanotechnology has become a transformative field in materials science, biomedical research, and environmental applications, offering solutions to long-standing challenges through the development of nanoscale materials with unique physical, chemical, and biological properties [1]. Among various nanomaterials, metal and metal oxide nanoparticles have gained increasing attention for their wide range of applications, particularly in antimicrobial, catalytic, and biomedical domains [2]. Copper oxide nanoparticles (CuO NPs), in particular, have demonstrated excellent antimicrobial, anticancer, and photocatalytic properties due to their high surface area-to-volume ratio, redox activity, and favorable electronic configuration [3]. Their ability to disrupt microbial membranes, generate reactive oxygen species (ROS), and interfere with intracellular metabolic pathways make them potent agents against a broad spectrum of pathogens [4].

Traditionally, CuO NPs have been synthesized through chemical and physical methods such as precipitation, hydrothermal, and sol-gel techniques [5]. However, these conventional approaches often require hazardous chemicals, high energy input, and extensive purification, raising concerns regarding environmental safety and biocompatibility [6]. In contrast, green synthesis methods, which utilize biological resources such as plant extracts, bacteria, fungi, or algae, offer eco-friendly, cost-effective, and sustainable alternatives [7]. These biological systems provide natural reducing and stabilizing agents such as proteins, polysaccharides, polyphenols, and alkaloids, which facilitate the synthesis of nanoparticles under mild conditions [8].

Among the biological agents employed in green synthesis, marine algae—especially brown algae belonging to the order Ectocarpales—have shown promise as effective sources of bioactive compounds [9]. Ectocarpales are known to contain a rich array of secondary metabolites including phenolics, flavonoids, polysaccharides, terpenoids, and chlorophyll derivatives, all of which can contribute to nanoparticle formation and stabilization [10]. These bioactive molecules not only aid in the reduction of metal ions to their nanoscale forms but also improve the biocompatibility and functional

properties of the resulting nanoparticles [11]. Furthermore, algae-mediated synthesis aligns with the principles of green chemistry, offering an environmentally responsible approach for the fabrication of functional nanomaterials [12].

The integration of biosynthesized nanoparticles into polymeric matrices opens new avenues for the fabrication of nanocomposite scaffolds, particularly in the biomedical field [13]. Electrospinning has emerged as a powerful technique to produce nanofibrous scaffolds with a high surface area, tunable porosity, and morphological similarity to the extracellular matrix (ECM), making them ideal for tissue engineering, wound healing, and drug delivery applications [14]. Polymers such as starch and polyvinyl alcohol (PVA) have been extensively used for scaffold fabrication due to their biocompatibility, biodegradability, and ease of processing [15]. Starch, a natural polysaccharide, offers excellent film-forming ability, while PVA contributes mechanical strength and flexibility [16]. When combined, starch/PVA blends can form robust electrospun fibers suitable for biomedical use [17].

Embedding nanoparticles such as CuO into these polymeric scaffolds can enhance their functional properties, particularly antimicrobial activity, which is critical for applications in wound care and infection control [18]. The presence of CuO NPs within the nanofibrous matrix can inhibit microbial colonization, prevent biofilm formation, and promote healing through local antimicrobial action [19]. Moreover, the uniform dispersion of nanoparticles within the scaffold can provide sustained release and improved interaction with biological systems [20]. Thus, the synergistic combination of biopolymer-based scaffolds and biologically synthesized CuO NPs presents a novel and effective strategy for the development of advanced biomaterials [21].

The current study was undertaken to explore the green synthesis of CuO NPs using aqueous extract derived from Ectocarpales [22], followed by their incorporation into starch/PVA-based electrospun nanofibrous scaffolds [23]. A series of physicochemical and morphological characterizations were conducted to confirm successful nanoparticle synthesis and scaffold fabrication [24]. UV–Visible spectroscopy was employed to monitor the optical behavior and surface plasmon resonance (SPR) of both the algal extract and synthesized CuO NPs [25]. Fourier-transform infrared spectroscopy (FT-IR) analysis provided insights into the functional groups involved in nanoparticle capping and scaffold matrix composition [26]. X-ray diffraction (XRD) was used to assess the crystalline structure and phase purity of the CuO NPs and nanocomposite scaffolds [27]. Scanning electron microscopy (SEM) offered detailed observations on particle size, shape, and scaffold morphology, revealing the successful embedding of nanoparticles into the fibrous matrix [28]. Thermogravimetric analysis (TGA) was used to evaluate the thermal stability of the scaffolds, an essential factor for biomedical and industrial applications [29]. In addition, dynamic light scattering (DLS) and zeta potential analyses were conducted to determine the size distribution and surface charge of the CuO NPs, which are key indicators of colloidal stability [30].

To further establish the functional potential of the developed materials, antimicrobial assays were performed against a panel of bacterial and fungal pathogens [31]. The green-synthesized CuO NPs and the electrospun nanofiber scaffolds were tested using agar well diffusion methods to assess their inhibitory effects [32]. The results demonstrated that while the algal extract and CuO NPs alone exhibited moderate antimicrobial activity, the CuO-loaded nanoscaffolds showed significantly enhanced performance [33]. The increased efficacy is attributed to the synergistic effects of the bioactive algal metabolites, the intrinsic antimicrobial nature of CuO, and the sustained release from the scaffold matrix [34].

This study contributes to the growing field of green nanotechnology by demonstrating a sustainable route for synthesizing CuO NPs using marine algae and applying them in functional biomaterials [35]. The use of Ectocarpales extract not only reduces the environmental footprint associated with chemical synthesis but also enhances the bioactivity of the resulting nanomaterials [36]. Moreover, the incorporation of CuO NPs into starch/PVA electrospun scaffolds represents a promising approach for developing multifunctional materials with high potential in biomedical, environmental, and pharmaceutical applications [37]. The comprehensive characterization of the synthesized nanoparticles and nanoscaffolds provides valuable insights into their structural, thermal, and biological attributes.

2. MATERIALS AND METHODS

2.1. Reagents and materials

This study employed marine brown algae (order Ectocarpales), collected from Rameswaram, Tamil Nadu, as a biological precursor for the eco-friendly synthesis of CuO NPs. Copper (II) sulfate pentahydrate (Sigma-Aldrich) served as the copper ion source. PVA (molecular weight 145,000) and commercially available starch were utilized to create nanofibrous scaffolds through electrospinning using the HOLMARC HO-NFES-040 setup. Solvents and chemicals of analytical grade from Merck and Sigma-Aldrich were employed without any additional purification. Characterization of materials involved techniques such as UV–Visible spectroscopy, FTIR, XRD (Bruker D8 Advance), SEM (JEOL JSM-IT800), zeta potential analysis (Malvern Zetasizer Ultra), and TGA (PerkinElmer TGA 8000).

2.2. Collection and processing of marine macroalgae

Marine brown algae from the Ectocarpales order were manually collected from the intertidal areas along the coastal region of Rameswaram. The algae were cleaned through sequential washing to remove contaminants such as sand, debris, and epiphytic organisms. Initially, the samples were rinsed thoroughly with tap water, followed by repeated washes with distilled water to eliminate remaining impurities. Approximately 100 grams of the clean biomass were chopped into smaller pieces and left to air dry at ambient temperature (~28°C) in a shaded area for 14 days. Once completely dried, the algae were ground using a mechanical grinder to obtain a fine, uniform powder, which was stored in airtight containers in dry conditions for subsequent use.

2.3. Ultrasonic-assisted extraction of bioactives

For extracting bioactive compounds, 2 grams of the powdered algae were added to 50 mL of Milli-Q water in a sterile 100 mL glass beaker. This mixture was subjected to ultrasonic-assisted extraction using a LABQUEST ultrasonic bath (Serial No. 941032329018, Borosil). The extraction was carried out at a steady temperature of 60°C for 45 minutes,

promoting cell wall disruption and release of intracellular compounds. The extract was then filtered using Whatman No. 1 filter paper under sterile conditions. The clear filtrate was collected and stored at 10°C for short-term use. For long-term preservation and further analysis, the extract was freeze-dried using a laboratory-scale lyophilizer, yielding a fine powdered form of the extract [38, 39].

2.4. Biosynthesis of CuO NPs

CuO NPs were synthesized through a green method involving the reduction of copper ions in the presence of bioactive compounds from the algal extract. Specifically, 50 mL of a 0.1 M aqueous solution of $CuSO_4 \cdot 5H_2O$ was combined with 10 mL of algal extract, prepared by dissolving 10 mg of freeze-dried material in 10 mL Milli-Q water. This blend, in a 5:1 volume ratio, was stirred continuously at 650 rpm on a magnetic stirrer and heated to 60°C for 2 hours. A visual color change from dark blue to pale greenish-blue indicated the initiation of CuO NPs formation. The colloidal solution was washed multiple times with double-distilled water to eliminate residual phytochemicals and unreacted metal ions. The final product was freeze-dried over 48 hours to produce CuO nanopowder, which was used for further characterization and integration into scaffolds [40].

2.5. Electrospinning of PVA/starch nanofibers loaded with CuO NPs

To generate composite nanofibers, an aqueous solution containing 15% (w/w) PVA was prepared by heating and stirring until complete dissolution. Starch (100 mg) and an equivalent quantity (100 mg) of green-synthesized CuO NPs were incorporated into the solution. This mixture was stirred at 50°C for 2.5 hours to ensure uniform dispersion. Electrospinning was performed using the HOLMARC HO-NFES-040 instrument. The blended polymer solution was loaded into a syringe fitted with a 0.84 mm inner-diameter needle. Electrospinning conditions were optimized: applied voltage was set to 11.5 kV, the distance from needle tip to collector was 12.3 cm, and the feed rate was maintained at 0.4 mL/h. The nanofibers were collected on grounded aluminum foil over a 6 to 8-hour period at room temperature to form continuous fibrous mats [41-43].

2.6. Physicochemical characterization

2.6.1. UV–visible spectroscopy

The absorbance profiles of the algal extract, synthesized CuO NPs, and PVA/starch/CuO nanofibers were analyzed using a VIS SPEC V-730 UV–Vis spectrophotometer. Absorbance was recorded across the 200–800 nm range, using deionized water as the baseline control [44].

2.6.2. FTIR spectroscopy analysis

Infrared spectral analysis was conducted on a PerkinElmer Spectrum Two FT-IR instrument operating in ATR mode. Spectra were recorded within 4000–400 cm^{-1} at a resolution of 4 cm^{-1}. To enhance signal clarity, each sample was scanned 64 times. The analysis helped identify functional groups responsible for nanoparticle biosynthesis and their interaction with the scaffold matrix [45].

2.6.3. XRD analysis

XRD was used to determine the crystalline nature of CuO NPs and nanofiber composites. A Bruker D8 Advance diffractometer was employed with CuKα radiation (λ = 1.5406 Å), operating at 40 kV and 40 mA. Data were collected across a 2θ range of 5°–90° with a step size of 0.029649°, providing detailed crystallographic information [46].

2.6.4. SEM analysis

Morphological characteristics and structural features of the CuO NPs and fabricated nanofibers were assessed using a JEOL JSM-IT800 SEM. Prior to imaging, samples were coated with a thin gold layer to enhance conductivity and image resolution. SEM analysis provided insight into fiber continuity, nanoparticle incorporation, and surface texture [47].

2.6.5. TGA

The thermal degradation behavior of nanofibrous scaffolds was evaluated using a PerkinElmer TGA 8000 system. Roughly 5 mg of each sample was placed in aluminum pans and heated from ambient temperature to 550°C at a constant rate of 15°C/min under nitrogen atmosphere. Weight loss data were used to assess thermal stability and decomposition phases [48].

2.6.6. Zeta potential and particle size analysis

Zeta potential and size distribution of CuO NPs were measured using a Malvern Zetasizer Ultra. DLS assessed hydrodynamic diameter, while electrophoretic light scattering determined zeta potential. These analyses provided valuable data on particle stability and dispersion in aqueous solutions [27].

Note: All raw characterization data supporting this research are publicly accessible via Mendeley Data (DOI: 10.17632/m7jzmb7mr9.1).

2.7. Antimicrobial activity analysis

The antimicrobial efficacy of Ectocarpales extract (50 µg/mL), green-synthesized CuO NPs (50 µg/mL), and starch/PVA-based electrospun nanofiber scaffolds (50 µg/mL) was evaluated using the agar well diffusion technique. Test organisms included Escherichia coli, Klebsiella pneumoniae, Staphylococcus aureus, Citrobacter koseri, Aspergillus niger, and Penicillium spp. Microbial cultures were adjusted to match the 0.5 McFarland standard and evenly spread over Mueller-Hinton agar for bacteria and Sabouraud dextrose agar for fungi. Wells of 6 mm diameter were carefully created under sterile conditions, into which 50 µL of each sample (50 µg/mL) and reference drugs—ciprofloxacin for bacteria and voriconazole for fungi—were introduced. Plates were allowed to pre-diffuse for 30 minutes before being incubated at 37°C for 24 hours (bacteria) and at 28°C for 48 hours (fungi). Post-incubation, the antimicrobial response was quantified by measuring the diameter (in mm) of the clear inhibition zones surrounding the wells. Greater inhibition zone sizes corresponded to enhanced antimicrobial effectiveness. All tests were performed in triplicate to ensure data consistency [49, 50].

2.8. Statistical evaluation

Data analysis was carried out using SPSS v25.0 and GraphPad Prism v9.0. All experiments were repeated in triplicates, and results were expressed as mean ± standard deviation. One-way ANOVA followed by Tukey's or Dunnett's post hoc test determined intergroup variations, with statistical significance defined at $p < 0.05$. The Shapiro–Wilk test evaluated data normality, and log transformation was applied where needed. Pearson's correlation was used to assess relationships between variables. A 95% confidence interval was used to ensure statistical robustness [51].

3. RESULTS

3.1. UV–visible spectroscopy

The UV–Visible spectral analysis (Figure 1) of the Ectocarpales extract and CuO NPs was carried out using a JASCO UV-VIS spectrophotometer (Model V-730), covering a wavelength range of 200–800 nm with deionized water as the blank. The Ectocarpales extract presented a broad UV absorption band within 200–400 nm, peaking at approximately 300 nm (0.93687 absorbance), indicative of π-π* transitions in compounds such as phenolics, flavonoids, or chlorophyll derivatives typical of algal sources. Beyond 400 nm, the visible region showed a gradual decrease in absorbance, implying limited chromophore presence [14]. Conversely, the CuO NPs exhibited a sharp UV absorption onset between 200–350 nm, with a maximum at 200 nm (0.53295), corresponding to electronic transitions and SPR. A steady reduction in absorbance was observed beyond this point, consistent with CuO NPs' optical features [15]. The clearly distinct absorption profiles between the extract and nanoparticles affirm their unique chemical natures—organic phytoconstituents in the extract and inorganic properties in CuO NPs—with no spectral overlaps. These findings support the successful synthesis and distinct optical characteristics of both samples, highlighting the algal metabolites' signature and the nanoparticulate inorganic framework.

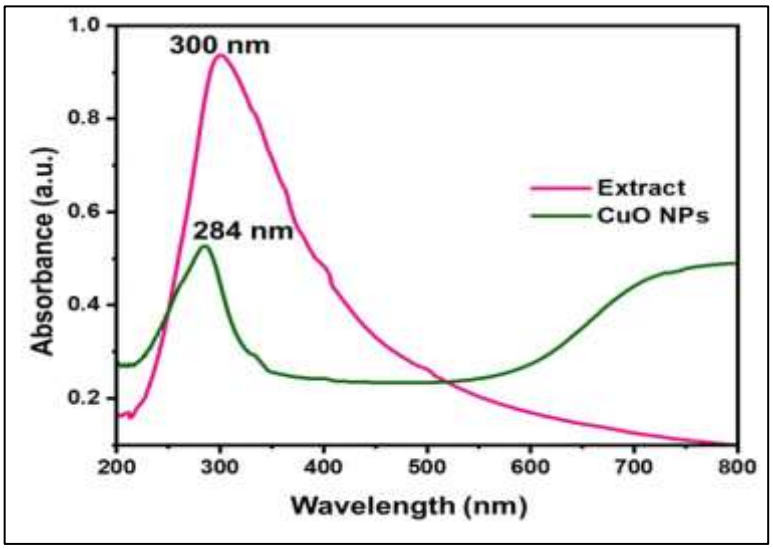

Figure 1. UV–Visible spectral profiles of algal extract and CuO NPs.

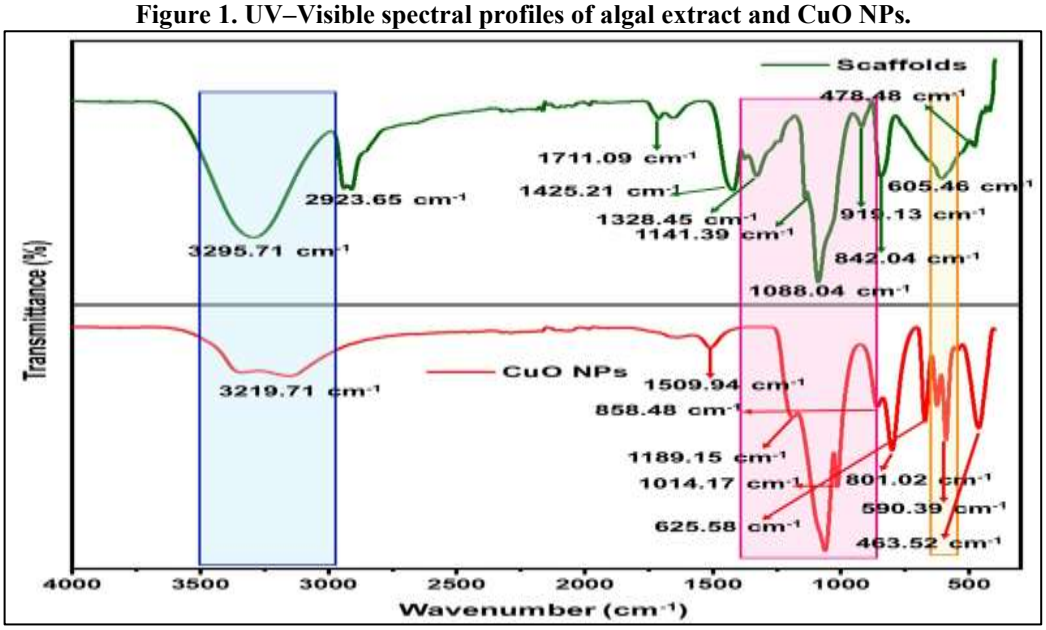

Figure 2. FTIR spectra of CuO NPs and their incorporation into nanoscaffolds.

3.2. FT-IR spectroscopy analysis

FT-IR spectra of CuO NPs and fabricated nanoscaffolds (Figure 2) were recorded using a PerkinElmer Spectrum Two instrument in ATR mode, covering the 4000–400 cm^{-1} range with a resolution of 4 cm^{-1} and 64 scans. The CuO NPs showed characteristic peaks at 3216 cm^{-1} (O–H stretching, likely due to adsorbed water), 1511 cm^{-1} (aromatic C=O

stretching or ring vibrations), and 860 cm^{-1} (Cu–O bond vibrations), validating the presence of metal-oxygen interactions and residual organic synthesis materials. On the other hand, nanoscaffolds exhibited distinct absorption bands at 3298 cm^{-1} (N–H/O–H stretching), 2107 cm^{-1} (weak C≡N or cumulative bond vibrations), 1652 cm^{-1} (carbonyl stretching), and 1327 cm^{-1} (C–N stretching or O–H bending), suggesting a complex matrix incorporating proteins, polysaccharides, or synthetic polymers. Additional bands at 840 and 607 cm^{-1} may denote glycosidic C–O–C linkages or inorganic contributions. The CuO NP sample revealed nine major peaks, while the nanoscaffolds exhibited eleven, reflecting greater complexity. These spectral data confirm successful CuO NP formation and a polymer-based scaffold structure facilitating nanoparticle embedding, with no overlapping signals, emphasizing their distinct molecular environments for biomedical utility.

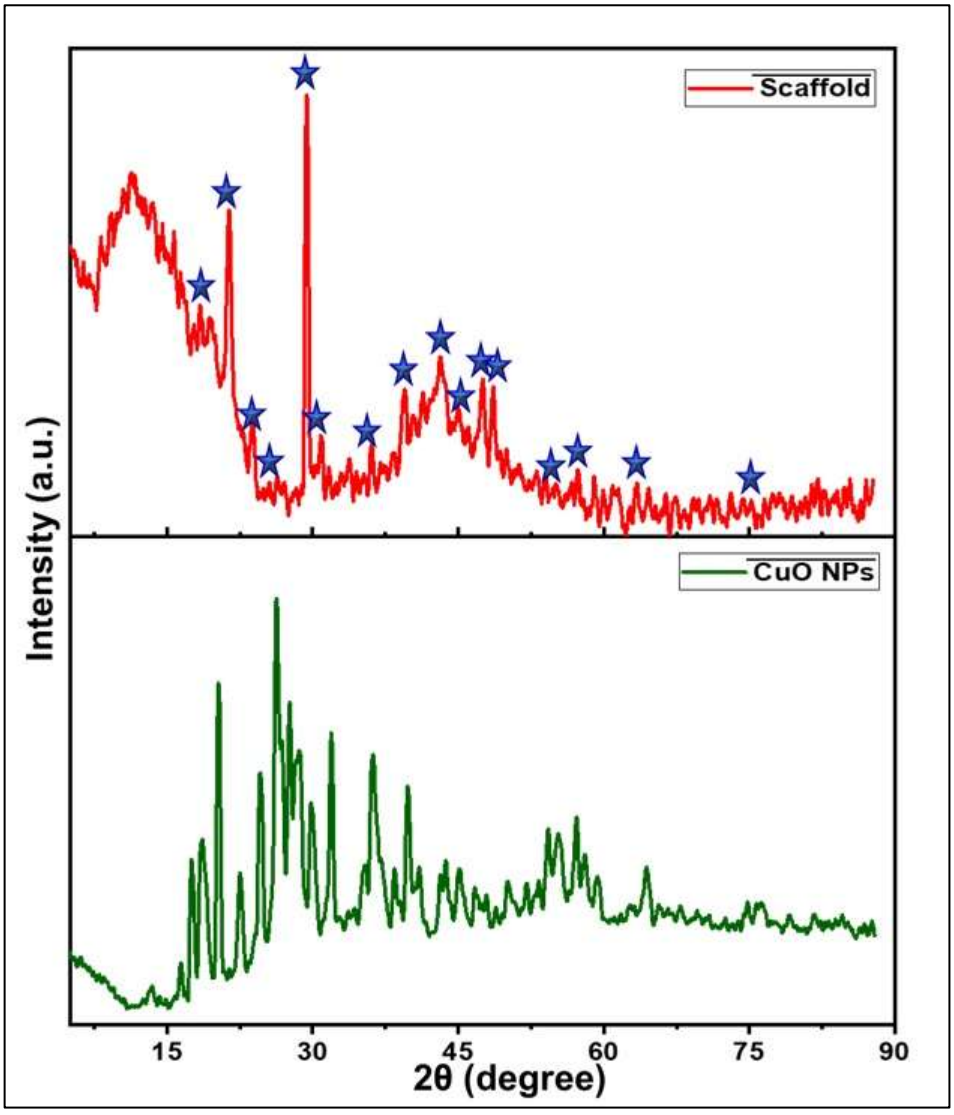

Figure 3. XRD patterns of synthesized CuO NPs and CuO-loaded scaffolds.

3.3. XRD analysis

XRD analysis (Figure 3) of CuO NPs and nanoscaffolds was performed using a Bruker D8 Advance diffractometer with CuKα radiation (λ = 1.5406 Å), operating at 40 kV and 40 mA, across a 2θ range of 5°–90° and step size of 0.029649°. CuO NPs revealed 25 diffraction peaks, notably at 26.201° (d = 3.398 Å, 100% intensity), 20.312° (d = 4.369 Å, 93.3%), and 36.148° (d = 2.483 Å, 45.3%), correlating with the monoclinic phase of tenorite CuO (JCPDS 05-0661). Narrow full-width half-maxima (e.g., 0.100° at 27.706° and 28.426°) and consistent d-spacings (1.268–5.449 Å) validated a highly crystalline structure. In contrast, nanoscaffolds exhibited 14 peaks, with strong reflections at 21.199° (d = 4.188 Å, 100%) and 30.844° (d = 2.897 Å, 82.5%), indicating a semi-crystalline polymer base (15.9% crystalline, 84.1% amorphous). Broader peaks (e.g., FWHM = 0.742° at 47.338°) and varied d-spacings (1.468–7.853 Å) reflected the scaffold's composite nature, likely due to polymer-CuO interactions. The lack of overlapping peaks between the two samples confirms structural purity—CuO NPs with sharp crystalline features and nanoscaffolds with hybrid amorphous-crystalline patterns—supporting successful synthesis and integration.

3.4. SEM analysis

SEM characterization (Figure 4) using a JEOL JSM-IT800 NANO SEM revealed distinct surface morphologies for CuO NPs and nanoscaffolds. The CuO NPs predominantly exhibited spherical to mildly irregular shapes, ranging from 50–200 nm in size, aligning with DLS results. High-resolution images showed slight aggregation likely due to surface charges, although many particles maintained discrete outlines. In contrast, electrospun nanoscaffolds displayed a porous, interconnected fibrous mesh with consistent diameters between 70–90 nm. The fibers appeared smooth with occasional bead formations, indicating controlled electrospinning. Embedded CuO NPs appeared as bright nano-protrusions along

fiber surfaces, confirming their integration into the polymer matrix. The 3D structure exhibited pores at both micro- and nanoscale, suitable for tissue regeneration or filtration uses. The lack of large NP clusters suggests effective dispersion, and the uniform fiber architecture reflects mechanical robustness. Collectively, these findings confirm the creation of CuO NP-loaded nanoscaffolds with optimized morphology and application potential in biomedical domains.

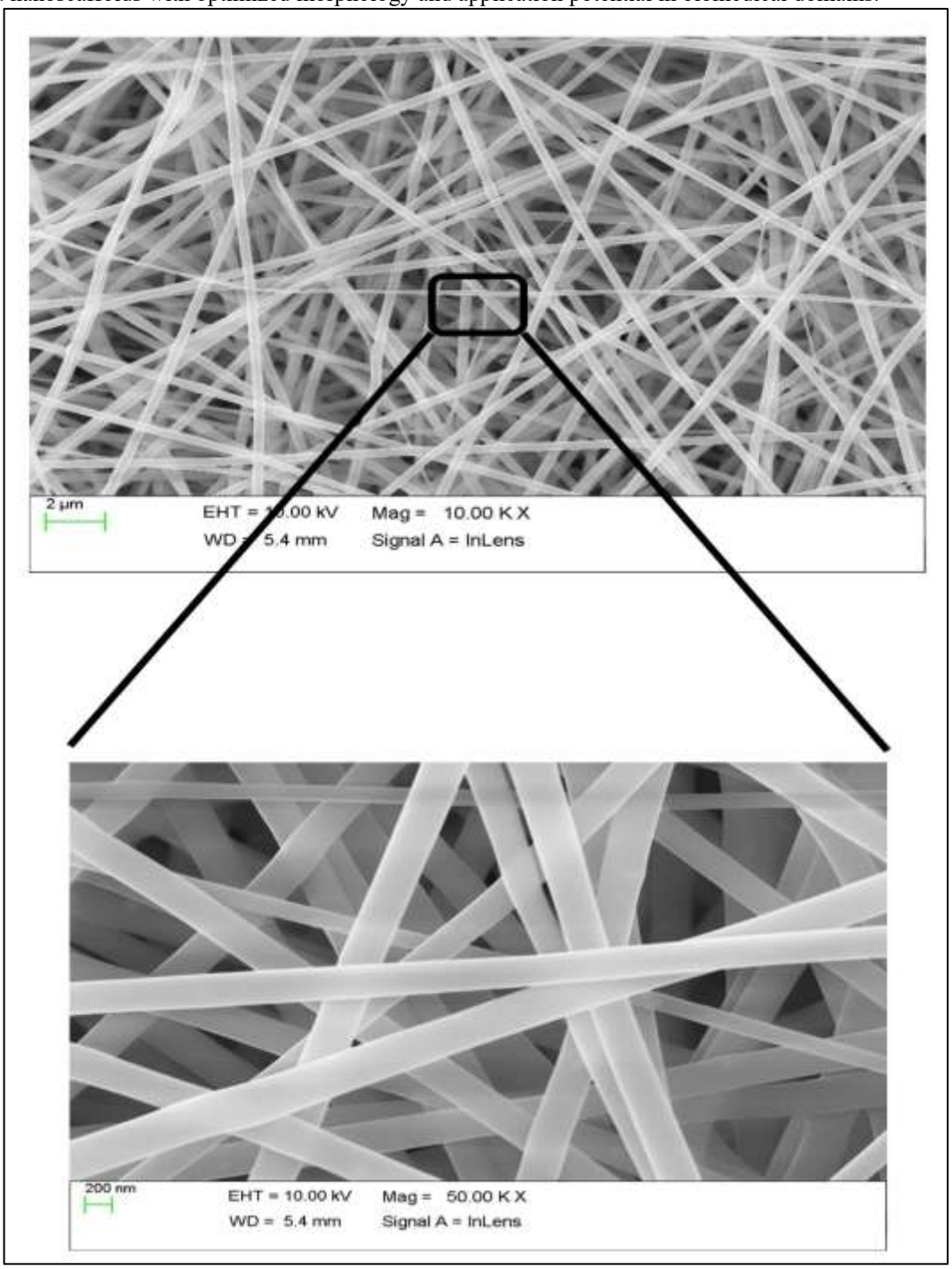

Figure 4. SEM analysis of starch/PVA/CuONPs nanoscaffolds

3.5. TGA

TGA of nanoscaffolds (Figure 5) was carried out using a PerkinElmer TGA 8000 under nitrogen with a 1.012 mg sample and a 15°C/min heating rate. A multi-step thermal degradation was observed, beginning at 238.41°C and peaking at 336.92°C, with complete breakdown by 400.84°C. The total weight loss of 31.102% up to 400°C suggested both organic (e.g., polymers) and inorganic content. Initial weight loss of 3.581% likely stemmed from moisture evaporation or residual solvents. A steep mass reduction centered at 336.92°C corresponded to polymer decomposition (e.g., starch/PVA chains), while the final residue confirmed the thermal durability of the inorganic CuO component. Minimal weight loss beyond 400°C indicates high thermal resilience, crucial for applications requiring heat stability. These results affirm the hybrid composition of the nanoscaffolds, combining polymer degradation profiles with the inert stability of metallic phases, endorsing their suitability for thermally demanding biomedical or environmental uses.

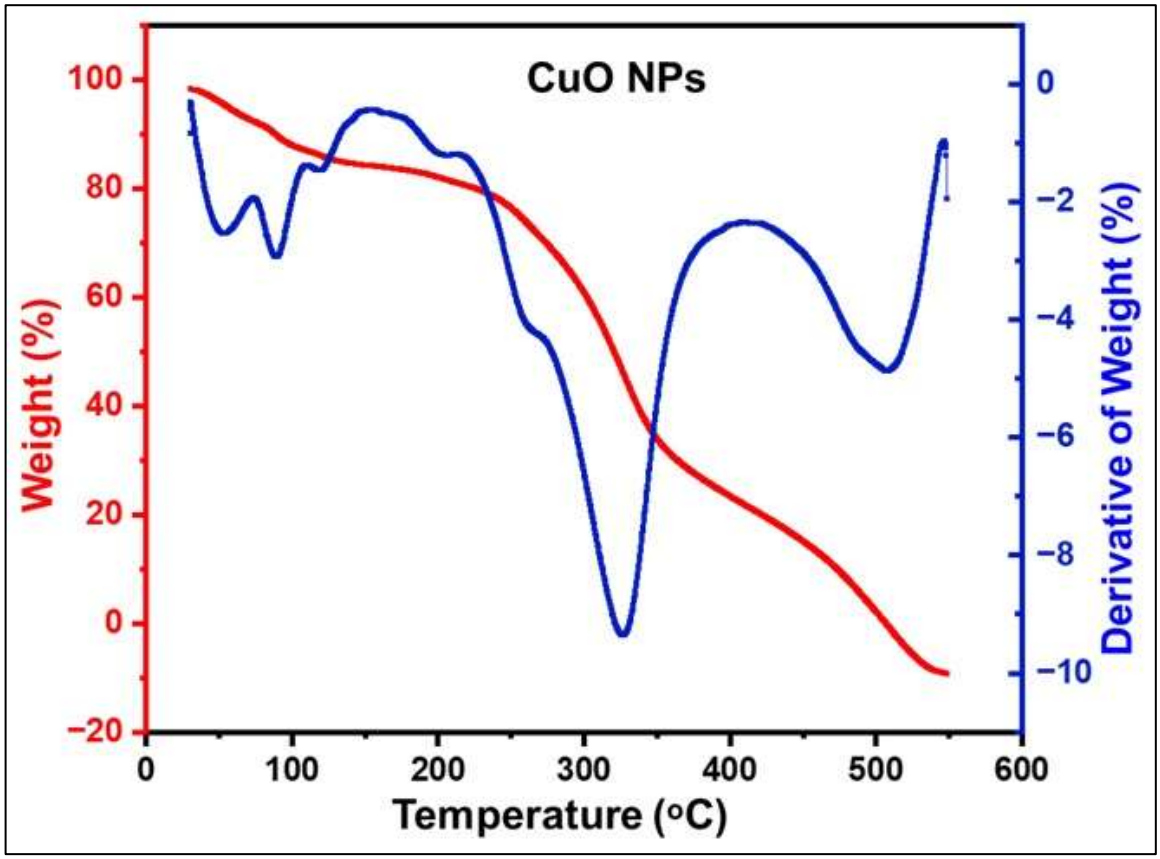

Figure 5. Thermal degradation behavior of CuO-incorporated nanoscaffolds.

3.6. Zeta potential and particle size analysis

DLS and zeta potential analysis of biosynthesized CuO NPs were conducted using a Malvern Zetasizer Ultra. The average particle size (Z-average) was 79.8 nm (Figure 6) with a polydispersity index (PDI) of 0.475, reflecting moderate size variability. Zeta potential averaged +14.03 mV, with distinct populations at +10.94 mV and +28.06 mV (Figure 7), indicative of positively charged surfaces. The system showed low conductivity (0.1179 mS/cm) and a quality factor of 2.084, pointing to stable dispersion. The presence of 5.5 µm aggregates indicates minor agglomeration. Overall, the CuO NPs displayed fair colloidal stability due to their positive charge, although further refinement in synthesis or dispersion might reduce aggregation. These characteristics are critical for performance in biological or environmental applications, where stability and uniform size distribution impact functionality.

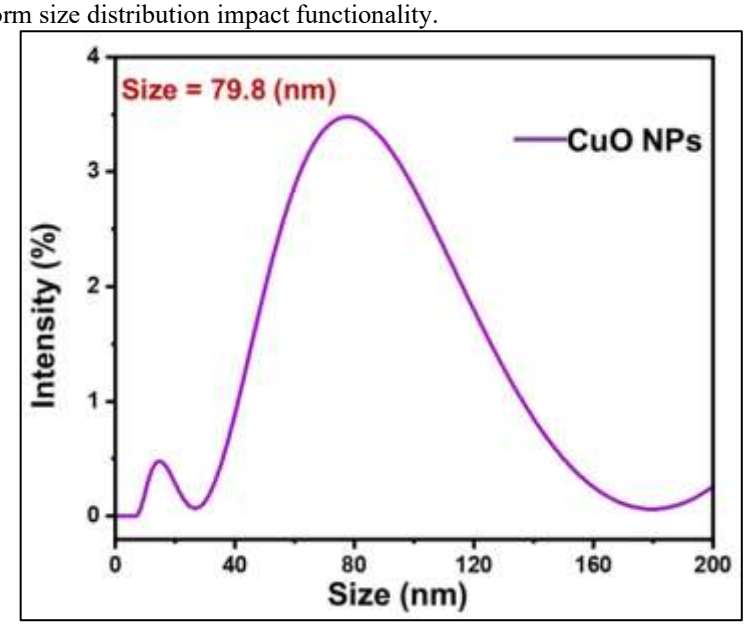

Figure6. DLS particles size analysis of CuO NPs

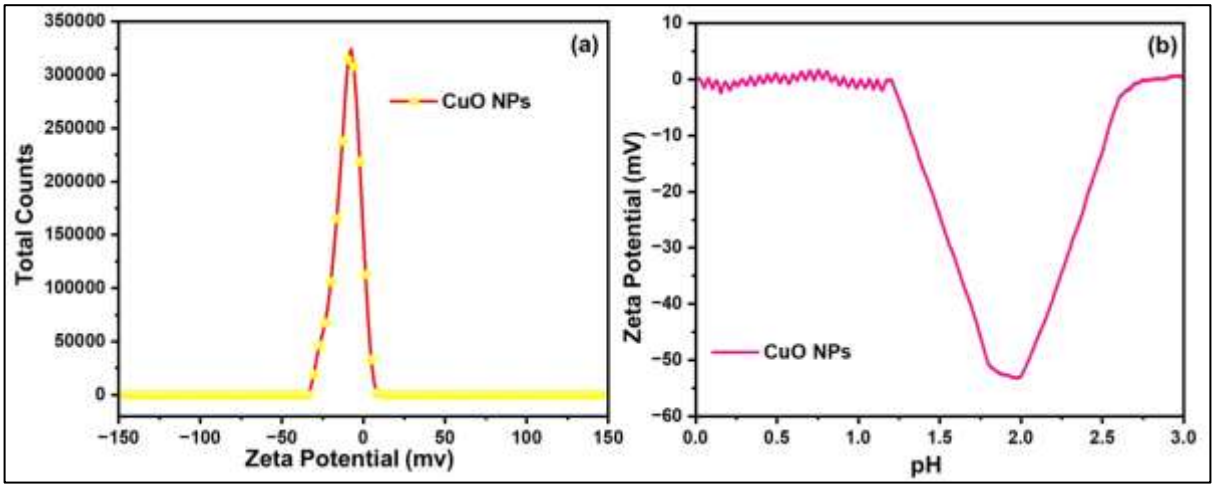

Figure7. Zeta-potential analysis of CuO NPs

3.7. Antimicrobial activity evaluation

The antimicrobial activity of Ectocarpales extract (50 µg/mL), green-synthesized CuO NPs (50 µg/mL), and starch/PVA-based electrospun nanofiber scaffolds (50 µg/mL) was assessed against bacterial and fungal pathogens using the agar well diffusion method (Table 1). The tested bacterial strains—Escherichia coli, Klebsiella pneumoniae, Staphylococcus aureus, and Citrobacter koseri—exhibited varying inhibition zones. The Ectocarpales extract demonstrated moderate activity, with zones of 17±0.12 mm, 16±0.36 mm, 15±0.27 mm, and 16±0.19 mm, respectively. CuO NPs showed lower efficacy, with inhibition zones of 22±0.29 mm, 21±0.18 mm, 19±0.28 mm, and 20±0.38 mm for the same bacteria. In contrast, the starch/PVA nanoscaffolds displayed strong antibacterial effects, with zones of 31±0.32 mm, 29±0.26 mm, 26±0.51 mm, and 27±0.52 mm, outperforming the algal extract and CuO NPs. For fungal pathogens—Aspergillus niger and Penicillium spp.—the algal extract produced zones of 14±0.17 mm and 15±0.38 mm, while CuO NPs showed zones of 17±0.18 mm and 19±0.26 mm. The nanoscaffolds again exhibited superior antifungal activity, with inhibition zones of 24±0.27 mm and 26±0.42 mm. The positive controls, ciprofloxacin (antibacterial) and voriconazole (antifungal), yielded higher inhibition zones (e.g., 33±0.58 mm for E. coli and 28±0.39 mm for Penicillium spp.), confirming the validity of the assay. All experiments were conducted in triplicate to ensure reproducibility, with the nanoscaffolds emerging as the most effective antimicrobial agent among the tested samples.

Table 1: Antimicrobial activity of Ectocarpales extract, CuO NPs, and starch/PVA electrospun nanoscaffolds at concentration of 50 µg/mL against various pathogenic organisms.

S. NO	ORGANISMS	ZONE OF INHIBITION (MM)				
		Ciprofloxacin (Antibiotic)	Voriconazole (Antifungal)	Algal Extract	CuO NPs	Nano-scaffolds
	Escherichia coli	33±0.58	-	17±0.12	22±0.29	31±0.32
	Klebsiella pneumoniae	30±0.14	-	16±0.36	21±0.18	29±0.26
	Staphylococcus aureus	28±0.32	-	15±0.27	19±0.28	26±0.51
	Citrobacter koseri	29±0.47	-	16±0.19	20±0.38	27±0.52
	Aspergillus niger	-	26±0.65	14±0.17	17±0.18	24±0.27
	Penicillium species	-	28±0.39	15±0.38	19±0.26	26±0.42

4. DISCUSSION

The synthesis and comprehensive characterization of CuO NPs and their integration into starch/PVA-based electrospun nanofibrous scaffolds were successfully achieved, as evidenced by various analytical techniques. The distinct physicochemical profiles derived from spectroscopic, microscopic, and diffraction studies underscore the efficacy of green synthesis using Ectocarpales extract and the successful fabrication of multifunctional nanoscaffolds for biomedical applications [52-56].

UV–Visible spectroscopy confirmed the presence of phytoconstituents in the Ectocarpales extract and the optical characteristics of CuO NPs [57]. The extract exhibited a broad absorption band around 300 nm, characteristic of π-π^* transitions commonly associated with phenolic or flavonoid compounds. These biomolecules likely served as reducing and stabilizing agents during nanoparticle synthesis [58]. In contrast, the CuO NPs displayed a sharp absorption peak at 200 nm, indicating strong SPR and validating nanoparticle formation. The absence of overlapping absorption bands between the extract and CuO NPs indicates the formation of discrete inorganic nanoparticles separate from organic biomolecules, demonstrating the transformation of bioactive metabolites into metal oxide nanostructures [59, 60].

FT-IR spectroscopy further elucidated the functional groups present in both the CuO NPs and the fabricated scaffolds. The CuO NPs showed prominent peaks related to O–H stretching, aromatic C=O groups, and Cu–O vibrations, confirming

the presence of residual organic molecules and metal-oxygen bonds. The electrospun nanoscaffolds, on the other hand, displayed additional peaks corresponding to amine, hydroxyl, carbonyl, and glycosidic linkages, suggesting the complex incorporation of polysaccharides and proteins from the Ectocarpales extract or scaffold matrix. The differences in peak patterns between the CuO NPs and nanoscaffolds reinforce the successful integration of nanoparticles into a biopolymer framework without chemical interference, thereby preserving their individual functionalities [61-65].

XRD analysis provided insights into the crystalline nature of the CuO NPs and the semi-crystalline structure of the nanoscaffolds. The CuO NPs exhibited distinct diffraction peaks that matched well with the standard monoclinic phase of tenorite CuO, demonstrating a high degree of crystallinity and structural purity. Conversely, the electrospun nanoscaffolds showed broader and fewer peaks, reflecting a predominantly amorphous polymeric base interspersed with crystalline CuO phases. The absence of peak overlap between CuO NPs and nanoscaffolds supports their successful integration while maintaining structural individuality. These findings are critical for applications where crystalline properties influence performance, such as in catalysis or antimicrobial efficacy [66, 67].

SEM further validated the morphological characteristics of both the CuO NPs and the nanofiber scaffolds. CuO NPs exhibited spherical to irregular morphologies within the nanoscale range (50–200 nm), with minor aggregation. This morphology is ideal for maximizing surface area and interaction with biological systems. The nanoscaffolds demonstrated a consistent fibrous mesh with diameters between 70–90 nm, containing embedded CuO NPs as surface protrusions. The uniform distribution of CuO NPs and the porous structure of the nanofibers suggest excellent mechanical stability and potential for applications such as wound healing or tissue engineering. The absence of large aggregates also indicates successful dispersion and interaction of CuO NPs within the polymer matrix [68, 69].

TGA of the nanoscaffolds demonstrated multi-stage thermal degradation with a significant decomposition peak at around 336.92°C, which is attributed to the breakdown of the polymeric chains. The initial mass loss likely corresponds to moisture evaporation, while the major weight reduction signifies degradation of the organic scaffold. The remaining residue implies the presence of thermally stable inorganic components like CuO. These results confirm the hybrid nature of the scaffold, blending biodegradable polymers with inorganic nanoparticles, and demonstrate their potential for biomedical applications requiring thermal stability, such as sterilization or high-temperature processing [70, 71].

DLS and zeta potential analyses revealed crucial information about the colloidal stability and size distribution of the biosynthesized CuO NPs. The trimodal size distribution, with an average hydrodynamic size of 79.8 nm and a PDI of 0.475, indicates moderate polydispersity, likely due to some nanoparticle aggregation. The zeta potential of +14.03 mV suggests a moderately stable colloidal system, where the positive surface charge prevents excessive agglomeration. However, the presence of larger aggregates highlights the need for optimizing synthesis or post-processing techniques to improve monodispersity. Such stability metrics are essential for biomedical applications, especially in drug delivery, where uniform nanoparticle behavior influences therapeutic efficacy [72-74].

The antimicrobial activity study offered compelling evidence of the functional superiority of the CuO NP-loaded nanoscaffolds. Although the Ectocarpales extract and CuO NPs individually exhibited moderate antibacterial and antifungal activity, the nanoscaffolds significantly outperformed both. The enhanced activity can be attributed to the synergistic effect of the embedded CuO NPs and the bioactive compounds present in the scaffold matrix. The scaffold's fibrous architecture may facilitate sustained release of antimicrobial agents and maximize surface interaction with microbial cells, leading to more effective pathogen inhibition. This is particularly evident in the larger inhibition zones observed against both Gram-positive and Gram-negative bacteria, as well as fungal strains [75, 76].

The combination of comprehensive spectroscopic, morphological, and biological assessments confirms the successful green synthesis of CuO NPs and their efficient incorporation into starch/PVA nanofibrous scaffolds. The distinct optical, structural, and functional properties of each component were preserved post-fabrication, resulting in a hybrid system with promising antimicrobial and biomedical potential. The nanoscaffolds, owing to their enhanced thermal stability, porous morphology, and superior antimicrobial efficacy, demonstrate great promise for applications in wound healing, antibacterial dressings, and other healthcare domains where multifunctional nanomaterials are essential.

5. CONCLUSION

This study successfully demonstrated the green synthesis of CuO NPs using Ectocarpales extract and their incorporation into starch/PVA-based electrospun nanofibrous scaffolds. UV–Visible spectroscopy confirmed the distinct optical properties of the algal extract and synthesized CuO NPs, while FTIR analysis revealed characteristic functional groups indicative of successful nanoparticle formation and scaffold fabrication. XRD patterns validated the crystalline nature of CuO NPs and the semi-crystalline structure of the nanoscaffolds. SEM analysis showed well-dispersed CuO NPs within a porous, fibrous scaffold matrix, suitable for biomedical applications. TGA results confirmed the thermal stability of the composite, while DLS and zeta potential analysis indicated moderate colloidal stability. Notably, antimicrobial assays revealed that the CuO NPs-loaded scaffolds exhibited enhanced antibacterial and antifungal activities compared to the extract and nanoparticles alone. Overall, the study highlights the potential of these bioengineered nanoscaffolds as effective antimicrobial agents for use in biomedical and environmental applications.

Ethical Declaration: Not applicable for this study.

Funding: Not available for this study.

Conflicts of Interest: The authors declare no conflicts of interest.

Data Availability Statement: The full dataset of physiochemical characterization associated with this work is published in Mendeley Data [Dataset] Structural and functional profiling of starch-polymer nanoscaffolds enhanced with Ectocarpales-

derived biogenic copper oxide nanoparticles (DOI: 10.17632/m7jzmb7mr9.1). Disclosure: The material characterization data and figures (e.g., UV, SEM, FTIR, XRD, TGA, Zeta Potential and particle sizer) presented here were generated from a common dataset and are being reused across multiple related studies on nanomaterials. All biological analyses and conclusions are original to each manuscript.

REFERENCES

1. Surendran N, Chandrasekaran G, Raju MV, Chandrasekaran MK, Ahalliya RM, Palanisamy CP, Kanniappan GV, Arcot R, Alharbi NS, Thiruvengadam M. Anti-inflammatory potential of ethanolic extract of Maranta arundinacea L.: Insights from COX-2 modulation and oxidative stress analysis. South African Journal of Botany. 2026; 195: 142-151.
2. Pei J, Senthilkumar MV, Hessini K, Subramaniyam S, Sivaramakrishnan R, Kanniappan GV, Jayaraman S, Palanisamy CP. Green fabrication of starch/PVA/CuO nanoscaffolds using marine macroalgae extract for enhanced anti-inflammatory activity. Sustainable Chemistry and Pharmacy. 2026; 51: 102397.
3. Balasubramanian V, Loganathan L, Muthuswamy K, Viswanathan TM, Raju MV, Chandrasekaran MK, Ahalliya RM, Poorasamy J, Palanisamy CP, Dominic S, Kanniappan GV. Anticancer therapeutic efficacy of PEGylated β-galactosidase from Aspergillus terreus in DMBA-induced breast cancer: Toxicological, molecular and histopathological evaluation in Wistar rats. International Journal of Biological Macromolecules. 2026; 360: 151856.
4. Jayaraman S, Eswaran A, Rajagopal P, Palanisamy CP, Veerakumar P, Veeraraghavan VP, Sirasanagandla SR. Neuroendocrine-associated epigenetic factors in cellular senescence: mechanisms and therapeutic implications. Biogerontology. 2026; 27(2): 64.
5. Ponnusamy B, Rajagopal P, Palanisamy CP, Veeraraghavan VP, Jayaraman S. Mechanistic Exploration of the anticancer activity of Justicia adhatoda Plant Leaf Ethanolic Extract against Colon Cancer Cells: An in silico and in vitro Approach. Asian Pacific Journal of Cancer Prevention. 2026; 27(3): 1069-1080.
6. Pei J, Saran VS, Sivaramakrishnan R, Kanniappan GV, Pandurangan V, Jayaraman S, Dhayalan VK, Mironescu M, Mironescu ID, Palanisamy CP. Ultrasonic-assisted, Sargassum ilicifolium (brown marine macroalgae)-mediated biogenic synthesis of CuO nanoparticles incorporated in starch/PVA electrospun nanoscaffolds: In vitro safety and antioxidant efficacy assessment. Bioorganic Chemistry. 2026; 173: 109679.
7. Raj MAPA, Subramaniyam S, Kanniappan GV, Jayaraman S, Palanisamy CP. Sustainable fabrication of starch/PVA/CuO electrospun nanoscaffolds from Turbinaria ornata (marine macroalgae) extract: Physicochemical characterization and antidiabetic evaluation. Kuwait Journal of Science. 2026; 53(2): 100545.
8. Pei J, Ganesh NS, Subramaniyam S, Sivaramakrishnan R, Kanniappan GV, Jayaraman S, Palanisamy CP. Sustainable fabrication of starch/PVA/CuO electrospun nanoscaffolds from Padina tetrastromatica (Brown macroalgae) extract: Physicochemical characterization and antidiabetic assessment. Sustainable Chemistry One World. 2026; 9: 100195.
9. Sakthiraj A, Sivaramakrishnan R, Subramaniyam S, Kanniappan GV, Pandurangan V, Jayaraman S, Dhayalan VK, Mironescu M, Mironescu ID, Palanisamy CP. Chemical Physics Impact. Starch/PVA electrospun nanoscaffolds loaded with ultrasonic-assisted green-synthesis of CuO nanoparticles from marine macroalgae (Gracilaria corticata) extract: Cytotoxicity and antioxidant analysis. 2026; 12: 101018.
10. Raju M, Chandrasekaran MK, Loganathan L, Ahalliya RM, Mironescu M, Mironescu ID, Palanisamy CP, Kanniappan GV. Lipid remodeling and ferroptosis in phosphatidylcholine-mediated tumor–stroma crosstalk. Frontiers in Molecular Biosciences. 2026; 13: 1742305.
11. Kunamalla R, Panagal M, Palanisamy CP. Biogenic synthesis and fabrication of starch/PVA/CuO electrospun nanoscaffolds from Sargassum ilicifolium (brown marine macroalgae) extract for anticancer activity on HT-29 and MCF-7 cancer cells. Biocatalysis and Agricultural Biotechnology. 2026; 72: 103923.
12. Pei J, Govindaraj H, Sivaramakrishnan R, Kanniappan GV, Pandurangan V, Dhayalan VK, Mironescu M, Mironescu ID, Jayaraman S, Palanisamy PC. Sustainable fabrication of biopolymer-based (starch/PVA) nanoscaffolds loaded with green-synthesized CuO nanoparticles from Sargassum wightii (marine macroalgae): Cytocompatibility and antioxidant activity. Biomaterials Advances. 2026; 182: 214660.
13. Pei J, Perumal NC, Meng P, Long Q, Palanisamy CP. Extracellular vesicle-based biosensors for Alzheimer's disease: A new frontier in precision diagnostics. Ageing Research Reviews. 2026; 113: 102904.
14. Shree P, Sivaramakrishnan R, Kanniappan GV, Pandurangan V, Jayaraman S, Dhayalan VK, Mironescu M, Mironescu ID, Palanisamy CP. Antioxidant and biocompatible CuO-starch/PVA nanoscaffolds via ultrasonic green synthesis using Turbinaria conoides (brown marine macroalgae). Medicine in Drug Discovery. 2025; 28: 100238.
15. Gong J, Lin J, Guan T, Pei J, Palanisamy CP, El-AtyFrom AMA. selenium tolerance to nanoplastic antagonism: Comprehensive characterization of L. casei SNUT1 and its extracellular vesicle–nanoselenium complex. Food Bioscience. 2025; 74: 107749.
16. Poochi SP, Sundarraj R, Raju MV, Chandrasekaran MK, Ahalliya RM, Palanisamy CP, Kanniappan GV, Kondapavuluri BK, Thiruvengadam M. Harnessing Nature: Computational and Experimental Insights Into Ipomoea obscura Metabolites for Bladder Cancer Therapy. Chemistry and Biodiversity. 2025; 0: e00909.
17. Dugganaboyana GK, Kannankumar MKG, Shivaramakrishna S, Raju MV, Chandrasekaran MK, Ahalliya RM, Panneerselvam N, Palanisamy CP, Kanniappan GV. Phytochemical insights, antioxidant activity and therapeutic potential of Cassia senna against prostate cancer in Wistar albino rats. Discover Applied Sciences. 2025; 7:1206.
18. Natarajan SR, Krishnamoorthy R, Alshuniaber MA, Gatasheh MK, Rajagopal P, Veeraraghavan VP, Palanisamy CP, Jayaraman S. KDM1A Facilitates Oncogenic Potential in Colorectal Cancer Progression Through the Activation of AXIN/GSK3β/β-Catenin Signaling Pathways: Evidence From Integrated Transcriptomics and In Vitro Studies. The Journal of Gene Medicine. 2025; 27(11): e70053.

19. Guan T, Gong J, Lin J, Palanisamy CP, Jinjin Pei J, El-Aty AMA. Machine learning-driven multimodal optimization of selenium biotransformation and flavor profiling in fermented apple–Yacon functional beverages. Innovative Food Science & Emerging Technologies. 2025; 105: 104198.
20. Natarajan SR, Krishnamoorthy R, Alshuniaber MA, Alsulami TS, Gatasheh MK, Rajagopal P, Palanisamy CP, Govindan R, Veeraraghavan VP, Jayaraman S. ABCE1 facilitates tumour progression via aerobic glycolysis and inhibits cell death in human colorectal cancer cells through the p53 signalling pathway. Scientific Reports. 2025; 15: 24674.
21. Huang Y, Guo H, Liu Y, Jin W, Palanisamy CP, Pei J, Oz F, El-Aty AMA. Effects of Natural Polysaccharides on the Gut Microbiota Related to Human Metabolic Health. Molecular Nutrition & Food Research. 2025; 69:e202400792.
22. Poornima K, Meenakshi K.C, Manikandan V.R, Shankari G, Prabhu D, Rathi M.A, Palanisamy CP, Balaji R, Gopalakrishnan V.K. Exploring the anticancer potential of Jerantinine A from Tabernaemontana coronaria against prostate, breast, and ovarian cancers: A computational approach. Journal of Complementary and Integrative Medicine, 2025 22(2): 363–372.
23. Palanisamy CP, Poompradub S, Sansanaphongpricha K, Jayaraman S, Subramani K. Faridah Sonsudin gGreen synthesis of Nigella sativa-mediated silver nanoparticles for enhanced antibacterial activity and wound healing: Mechanistic insights and biomedical applications. Environmental Nanotechnology, Monitoring & Management. 2025; 24: 101085.
24. Surendran N, Raju MV, Chandrasekaran MK, Ahalliya RM, Palanisamy CP, Chandrasekaran G, Kanniappan GV. Physicochemical characterization of starch from Maranta arundinacea L.(arrowroot) rhizomes and its inhibition of COX-2: In vivo validation. Bioactive Carbohydrates and Dietary Fibre. 2025; 33: 100465.
25. Kannappan P, Chandrasekaran MK, Raju MV, Gopalakrishnan S, Dhamodharan P, Ahalliya RM, Palanisamy CP, Raju B, Kanniappan GV. Exploring the anticancer potential of Jerantinine A from Tabernaemontana coronaria against prostate, breast, and ovarian cancers: a computational approach. Journal of Complementary and Integrative Medicine. 2025; 22(02): 363-372.
26. Pei J, Kumarasamy RV, Jayaraman S, Kanniappan GV, Long Q, Palanisamy CP. Quercetin-functionalized nanomaterials: Innovative therapeutic avenues for Alzheimer's disease management. Ageing Research Reviews. 2025; 104: 102665.
27. Jayaraman S, Prasad M, Natarajan SR, Krishnamoorthy R, Alshuniaber MA, Gatasheh MK, Veeraraghavan VP, Rajagopal P, Palanisamy CP. Molecular mechanisms underlying the effects of beta-sitosterol on TGF-β1/Nrf2/SIRT1/p53-mediated signaling in the kidney of a high-fat diet and sucrose-induced type-2 diabetic rat. Chemico-Biological Interactions. 2025; 411: 111443.
28. Huang Y, Guo H, Liu Y, Jin W, Palanisamy CP, Pei J, Oz F, El-Aty AMA. Effects of Natural Polysaccharides on the Gut Microbiota Related to Human Metabolic Health. Molecular Nutrition & Food Research. 2025; e202400792.
29. Prabhakaran P, Palanisamy CP, Shanmugam A, Damodharan P, Swaminathan H, Devaraj D, Ahalliya RM, Kanniappan GV. Isolation, structural characterization, and molecular docking studies on the bioactive compound from n-Hexane extract of Emilia sonchifolia (L.) DC against the pancreatic cancer target Aurora 2 Kinase. Journal of Complementary and Integrative Medicine. 2024; 22(1): 0290.
30. Jiang H, Kumarasamy RV, Pei J, Raju K, Kanniappan GV, Palanisamy CP. Integrating engineered nanomaterials with extracellular vesicles: Advancing targeted drug delivery and biomedical applications. Frontiers in Nanotechnology. 2024; 6: 1513683.
31. Natarajan PM. Dental Bioinformnatics-Current Scope and Future perspectives. Research Journal of Pharmacy and Technology. 2022;15(5):2351-6.
32. Vidhyarekha U, Natarajan PM, Bhuminathan S, Sabarinathan J, Suba R, Vijayalakshmi P. Role of artificial intelligence in Oral Cancer. Advances in Public Health. 2024. 2024: 3664408.
33. Ganesan A, Kumar NG, Natarajan PM, Gauthaman J. Automated classification of elongated styloid processes using deep learning models-an artificial intelligence diagnostics. Frontiers in Oral Health. 2025; 5: 1424840.
34. Umapathy VR, Natarajan PM, Swamikannu B. Regenerative Strategies in Dentistry: Harnessing Stem Cells, Biomaterials and Bioactive Materials for Tissue Repair. Biomolecules. 2025; 15: 546.
35. Natarajan PM, Umapathy VR, Murali A, Swamikannu B. (2022). Computational Simulations of Identified marine-derived Natural Bioactive Compounds As Potential Inhibitors of Oral Cancer. Future Science OA. 2022; 8(3).
36. Ganesan A, Kumar NG, Natarajan PM. Solanum trilobatum leaf extract-derived silver nanoparticles downregulate the PI3K/AKT/mTOR signaling pathway and attenuate oral squamous cell carcinoma cell proliferation. Journal of Herbmed Pharmacology. 2024; 13(2): 300-307.
37. Perumal MKK, Renuka RR, Subbiah SK, Natarajan PM. Artificial intelligence-driven clinical decision support systems for early detection and precision therapy in oral cancer: a mini review. Frontiers in Oral Health. 2025; 6: 1592428.
38. Ramesh E, Ganesan A, Lakshmi KC, Natarajan PM. Artificial intelligence-based diagnosis of oral leukoplakia using deep convolutional neural networks Xception and MobileNet-v2. Frontiers in Oral Health. 2025; 6: 1414524.
39. Natarajan PM. Computational Studies on Recent Congeners of Fluoroquinolones and Nitroimidazoles for Their Use in Periodontal Therapy. Journal of Pharmacy and Bioallied Sciences. 2024; 16(5): S4731-S4740.
40. Ganesan A, Kumar NG, Natarajan PM. Anticancer activity of silver nanoparticles synthesized from aqueous leaf extract of Solanum trilobatum (Purple fruit pea eggplant) on human oral cancer cells. Journal of Herbmed Pharmacololgy. 2024; 13(2): 260-268.
41. Umapathy V, Dhanavel A, Kesavan R, Natarajan PM, Bhuminathan S, Vijayalakshmi P. Anticancer Potential of the Principal Constituent of Piper nigrum, Piperine: A Comprehensive Review. Cureus. 2024; 16(2): e54425.
42. Natarajan PM, Bhuminathan S, Rajan R, Bindu K, Loganathan K, Veerakumar R. The Crucial Role of Smoking Cessation in Preventing Oral Cancer. Journal of Pharmacy and Bioallied Sciences. 2024; 16(5): S4245-S4247.

43. Umapathy VR, Swamikannu B, Natarajan PM, Devi R, Nandini MS, Vimalarani, Vijayalakshmi P. In Silico Molecular Docking of Ocimum sanctum Phytochemicals: Targeting Key Biomarkers in Oral Cancer. Journal of Pharmacy and Bioallied Sciences. 2024; 16(5): S4792-S4799.
44. Natarajan PM, Umapathy VR. Role of transcriptomics in the study of oral cancer. Frontiers in Oral Health. 2025; 6:1524364.
45. Swamikannu B, Umapathy VR, Natarajan PM, Nandini MS, Stylin AGSQ, Vimalarani V, Rajinikanth S. Unlocking the Therapeutic Benefits of Artemisia Annua: A Comprehensive Overview of its Medicinal Properties. Journal of Pharmacy and Bioallied Sciences. 2024; 16(5): S4248-S4253.
46. Yadalam PK, Arumuganainar D, Natarajan PM, Ardila CM. Artificial intelligence-powered prediction of AIM-2 inflammasome sequences using transformers and graph attention networks in periodontal inflammation. Scientific Reports. 2025; 15: 8733.
47. Yadalam PK, Chatterjee S, Natarajan PM, Ardila CM. Comparison of light gradient boosting and logistic regression for interactomic hub genes in Porphyromonas gingivalis and Fusobacterium nucleatum-induced periodontitis with Alzheimer's disease. Frontiers in Oral Health. 2025; 6:1463458.
48. Natarajan PM, Bhuminathan S, Leela B, Bindu K, Loganathan K, Ramachandran V. Smoking and its Role in Oral Cancer. Journal of Pharmacy and Bioallied Sciences 16(5): S4242-S4244.
49. Yadalam PK, Natarajan PM, Ardila CM. Variational graph autoencoder for reconstructed transcriptomic data associated with NLRP3 mediated pyroptosis in periodontitis. Scientific Reports. 2025; 15: 1962.
50. Natarajan PM, Swamikannu B, Sivaraman NM, Stylin AGSQ. Prevention of Oral Cancer: A Comprehensive Guide. Journal of Pharmacy and Bioallied Sciences. 2024; 16(5): S4239-S4241.
51. Guo H, Liu Y, Wan T, Song D, Palanisamy CP, Geng J, Pei J, Özmen S, El-Aty AMA. Toward personalized cancer management: Role of precision nutrition–diet interventions. Journal of Functional Foods. 2024; 123: 106584.
52. Natarajan SR, Krishnamoorthy R, Alshuniaber MA, Al-Anazi KM, Farah MA, Rajagopal P, Palanisamy CP, Veeraraghavan VP, Jayaraman S. Identification of FOXM1 as a novel protein biomarker and therapeutic target for colorectal cancer progression: Evidence from immune infiltration and bioinformatic analyses. International Journal of Biological Macromolecules. 282 (Part 4): 137201.
53. Rajendran MS, Jayaraman S, Khan JM, Jasmine S, Prabhakaran RK, Raju MV, Chandrasekaran MK, Ahalliya RM, Kannappan P, Palanisamy CP, Kanniappan GV. Investigating the colon toxicity and carcinogenic role of monosodium glutamate compared with Dimethylhydrazine in male Wistar rats: Exploring the link to childhood colon cancer risk. Journal of King Saud University - Science. 2024; 36(11): 103507.
54. Kumarasamy RV, Natarajan PM, Umapathy VR, Roy JR, Rab SO, Saeed M, Panagal M, Mironescu M, Srinivasan GP, Palanisamy CP. Clinical Applications and Therapeutic Potentials of Advanced Nanoparticles: A Comprehensive Review on Completed Human Clinical Trials. Frontiers in Nanotechnology. 2024; 6:1479993.
55. Jin W, Pei JJ, Roy JR, Jayaraman S, Ahalliya RM, Kanniappan GV, Mironescu M, Palanisamy CP. Comprehensive review on single-cell RNA sequencing: A new frontier in Alzheimer's disease research. Ageing Research Reviews. 2024; 274: 102454.
56. Pei J, Palanisamy CP, Jayaraman S, Natarajan PM, Umapathy VR, Roy JR, Panagal M, Jayaraman S. Curcumin-loaded polymeric nanomaterials as a novel therapeutic strategy for Alzheimer's disease: A comprehensive review. Ageing Research Reviews. 2024; 99: 102393.
57. Pei J, Palanisamy CP, Jayaraman S, Natarajan PM, Umapathy VR, Roy JR, Thalamati D, Ahalliya RM, Kanniappan GV*, Mironescu M. A comprehensive review on starch-based Sustainable Edible Films Loaded with Bioactive Components for Food Packaging. International Journal of Biological macromolecules. 2024; 274 (Part-1): 133332.
58. Palanisamy CP, poompradub S, Sansanaphongpricha K, Subramani K, Sonsudin F. Increased expression levels of PDGF and VEGF magnify the wound healing potential facilitated by biogenic synthesis of silver nanoparticles. Nano-Structures & Nano-Objects. 2024; 39: 101236.
59. Pei J, Palanisamy CP, Jayaraman S, Natarajan PM, Umapathy VR, Roy JR, Thalamati D, Ahalliya RM, Kanniappan GV, Mironescu M. Proteomics Profiling of Extracellular Vesicle for Identification of Potential Biomarkers in Alzheimer's Disease: A Comprehensive Review. Ageing Research Reviews. 2024; 99: 102359.
60. Xi J, Wang T, Xian P, Liu X, Du M, Yang H, Palanisamy CP, Lin W, Long Q. Proteomic insights uncover enhanced neurotherapeutic potential in conditioned mesenchymal stem cell-derived extracellular vesicles. Extracellular Vesicle. 2024; 3: 100037.
61. Pei J, Natarajan PM, Umapathy VR, Swamikannu B, Sivaraman NM, Krishnasamy L, Palanisamy CP. Advancements in the synthesis and functionalization of zinc oxide-based nanomaterials for enhanced oral cancer therapy. Molecules. 2024; 29(11): 2706.
62. Gatasheh MK, Natarajan SR, Krishnamoorthy R, Alsulami TS, Rajagopal P, Palanisamy CP, Veeraraghavan VP, Jayaraman S. Molecular analysis to identify novel potential biomarkers as drug targets in colorectal cancer therapy: an integrated bioinformatics analysis. Molecular and Cellular Oncology. 2024; 11(1): 2326699.
63. Pei J, Yan Y, Jayaraman S, Rajagopal P, Natarajan PM, Umapathy VR, Gopathy S, Roy JR, Sadagopan CS, Thalamati D, Palanisamy CP, Mironescu M. A review on advancements in the application of starch-based nanomaterials in biomedicine: Precision drug delivery and cancer therapy. International Journal of Biological Macromolecules. 2024; 130746.
64. Pei JJ, Yan Y, Palanisamy CP, Jayaraman S, Natarajan PM, Umapathy VR, Gopathy S, Roy JR, Sadagopan JC, Thalamati D, Mironescu M. Materials-based drug delivery approaches: Recent advances and future perspectives. Green Processing and Synthesis. 2024; 13: 20230094.

65. Panneerselvam S, Viswaja K, Deepa E, Prathiba S, Rebecca FS, Nivedha RP, Rajagopal P, Veeraraghavan VP, Sridevi G, Palanisamy CP, Jayaraman S. Hypoglycemic Potential of Acalypha indica in Streptozotocin-Induced Type 2 Diabetic Rats. International Journal of Drug Delivery Technology. 2026; 16(26s):1038-1047.
66. Panneerselvam S, Viswaja K, Prathiba S, Rebecca FS, Nivedha RP, Rajagopal P, Fathima SJH, Veeraraghavan VP, Sridevi G, Palanisamy CP, Jayaraman S. Acalypha Indica Attenuates Insulin Resistance in STZ-Induced Type 2 Diabetic Male Rats: Mechanistic Study. International Journal of Drug Delivery Technology. 2026; 16(26s):1027-1037.
67. Manju NE, Natarajan A, Rebecca FS, Nivedha RP, Hemalatha R, Rajagopal P, Murali R, Veeraraghavan VP, Sridevi G, Palanisamy CP, Jayaraman S. Effect of Seendhil polyherbal formulation in attenuating type-2 diabetes in STZ-induced experimental rats. International Journal of Drug Delivery Technology. 2026; 16(26s):981-989.
68. Manju NE, Natarajan A, Rebecca FS, Nivedha RP, Hemalatha R, Rajagopal P, Murali R, Veeraraghavan VP, Sridevi G, Palanisamy CP, Jayaraman S. Molecular mechanism to identify the effects of Seendhil polyherbal preparation on IRS-1/AKT/GLUT4/NRF2-KEAP-1 mediated signaling in SFZ-induced type-2 diabetic adult male rats. International Journal of Drug Delivery Technology. 2026;16(26s):972-980.
69. Palanisamy CP, Poompradub S, Sansanaphongpricha K, Jayaraman S, Subramani K, Sonsudin F. Biosynthesis of silver nanoparticles (AgNPs) using ethanolic extract of Nigella sativa (L.) seeds promotes wound healing via PDGF and VEGF signalling pathways activation. Biocatalysis and Agricultural Biotechnology. 2023; 54: 102970.
70. Palanisamy CP, Pei JJ, Phaniendra A, Venkata AAN, Jayaraman S, Veeraragahavan VP, Sridevi G, Roy JR, Janaki CS, Thalamati D, Mironescu M, Luo Q, Chai Y, Long Q. New Strategy of Neurodegenerative Disease Treatment with Extracellular Vesicles (EVs) Derived from Mesenchymal Stem Cells (MSCs). Theranostics. 2023; 13(12):4138-4165.
71. Singh N, Kumar B, Usman UL, Susan MABH. Nano revolution: exploring the frontiers of nanomaterials in science, technology, and society. Nano-Structures & Nano-Objects. 2024;39:101299.
72. Nikolova MP, Chavali MS. Metal oxide nanoparticles as biomedical materials. Biomimetics. 2020;5(2):27.
73. Saleem MH, Ejaz U, Vithanage M, Bolan N, Siddique KH. Synthesis, characterization, and advanced sustainable applications of copper oxide nanoparticles: a review. Clean Technologies and Environmental Policy. 2024:1-26.
74. Li H, Zhou X, Huang Y, Liao B, Cheng L, Ren B. Reactive oxygen species in pathogen clearance: the killing mechanisms, the adaption response, and the side effects. Frontiers in microbiology. 2021;11:622534.
75. Siddiqui H, Parra MR, Haque FZ. Optimization of process parameters and its effect on structure and morphology of CuO nanoparticle synthesized via the sol− gel technique. Journal of Sol-Gel Science and Technology. 2018;87:125-35.
76. Ahmed S, Mofijur M, Nuzhat S, Chowdhury AT, Rafa N, Uddin MA, et al. Recent developments in physical, biological, chemical, and hybrid treatment techniques for removing emerging contaminants from wastewater. Journal of hazardous materials. 2021;416:125912.